



Publication Year	2018
Acceptance in OA @INAF	2021-04-19T16:16:10Z
Title	Identification of activity peaks in time-tagged data with a scan-statistics driven clustering method and its application to gamma-ray data samples
Authors	PACCIANI, LUIGI
DOI	10.1051/0004-6361/201732115
Handle	http://hdl.handle.net/20.500.12386/30803
Journal	ASTRONOMY & ASTROPHYSICS
Number	615

Identification of activity peaks in time-tagged data with a scan-statistics driven clustering method and its application to gamma-ray data samples¹

L. Pacciani¹

Istituto di Astrofisica e Planetologia Spaziali - Istituto Nazionale di Astrofisica (IAPS-INAF), Via Fosso del Cavaliere, 100 - I-00133 Rome (Italy)
e-mail: luigi.pacciani@iaps.inaf.it

August 27, 2018

ABSTRACT

Context. The investigation of activity periods in time-tagged data samples is a topic of large interest. Among Astrophysical samples, gamma-ray sources are widely studied, due to the huge quasi-continuum data set available today from the FERMI-LAT and AGILE-GRID gamma-ray telescopes.

Aims. To reveal flaring episodes of a given gamma-ray source, researchers make use of binned light-curves. This method suffers several drawbacks: the results depends on time-binning, the identification of activity periods is difficult for bins with low signal to noise ratio. A different approach is investigated in this paper.

Methods. I developed a general temporal-unbinned method to identify flaring periods in time-tagged data and discriminate statistically-significant flares: I propose an event clustering method in one-dimension to identify flaring episodes, and Scan-statistics to evaluate the flare significance within the whole data sample. This is a photometric algorithm. The comparison of the photometric results (e.g., photometric flux, gamma-ray spatial distribution) for the identified peaks with the standard likelihood analysis for the same period is mandatory to establish if source-confusion is spoiling results.

Results. The procedure can be applied to reveal flares in any time-tagged data sample. The study of the gamma ray activity of 3C 454.3 and of the fast variability of the Crab Nebula are shown as examples. The result of the proposed method is similar to a photometric light curve, but peaks are resolved, they are statistically significant within the whole period of investigation, and peak detection capability does not suffer time-binning related issues.

The method can be applied for gamma-ray sources of known celestial position, for example, sources taken from a catalogue. Furthermore the method can be used when it is necessary to assess the statistical significance within the whole period of investigation of a flare from an unknown gamma-ray source.

Key words. gamma-ray: general – methods: statistical – methods: data-analysis – gamma-ray flare – unbinned light curve – Scan Statistics – time-tagged data

1. Introduction

The study of source variability is a fundamental topic in Astrophysics. I treat here the problem of peak activity identification in time-tagged data samples. This study is primary motivated by the huge Fermi-LAT and AGILE archival data sample.

The Fermi Satellite operations allow for each position of the sky to be observed every orbit or two, and in some case every 4 orbits of the satellite around the Earth. This strategy is operating for the entire observation period (9 years, up to now) of the FERMI-LAT pair production gamma-ray telescope (Atwood 2009).

AGILE (Tavani 2009) also operates in spinning mode and scan the whole sky every ~ 7 minutes.

These scanning-sky strategies allow researcher to study gamma-ray variability of Celestial Sources for the whole Missions lifetime, without gaps.

The two preferred methods of investigation are likelihood

analysis (Mattox 1996) and binned light-curves.

The Likelihood analysis, can be applied for a fixed integration period, such as for the preparation of a catalog, or for the observation of a field within a predefined period.

The binned light-curve analysis is the preferred method to investigate source variability. It introduces an obvious timescale (the time-bin). Several light curves (varying time-bin and bin positions) are usually applied to data to recognize flares, their duration, and peak activity. The statistical significance for every bin of the light curves is evaluated. It refers to the significance of source signal against background within the chosen time-bin. False flare detection post-trial probability (P_{false}) can be evaluated (see, e.g., Bulgarelli 2012) in order to study significance of the flaring activity period against background statistical fluctuations during the whole period of investigation. The evaluated P_{false} can be used when mean source signal is negligible with respect to background within the whole scrutinized period.

Lott (2012) proposes an adaptive light curve strategy to overcome the drawbacks arising from a fixed time-bin.

An other method to study gamma-ray source variability from the FERMI-LAT data sample is investigated in Ackerman (2013).

¹ C code implementing the whole procedure and supplementary material is available in electronic form at the CDS via anonymous ftp to cdsarc.u-strasbg.fr (130.79.128.5) or via <http://cdsweb.u-strasbg.fr/cgi-bin/qcat?J/A+A/>.

Scan-statistics (Naus 1965) evaluates statistical significance of the maximum number of events found within a moving window of fixed length (see Wallenstein 2009, for a review). It is the natural approach to study the statistical significance of detection of non-random clusters against the hypothesis of an uniform distribution on an interval. Naus (1966) obtained that the power of scan-test is larger with respect to disjoint-test (e.g., with respect to binned light curve investigation) assuming to know the cluster size. Nagarwalla (1996); Glaz & Zhang (2006) investigated the case of an unknown cluster size, but the results of their methods depend on several hypothesis.

Cucala (2008) studied an hypothesis-free method based on the distance $D_{i,j} = X_{(j)} - X_{(i)}$ among ordered events i, j where $X_{(i)}$ is the position of the event of index i in the extraction interval. I propose here a similar clustering method to identify activity periods above an assumed uniformly distributed data sample. It allows to obtain unbinned light curves of astrophysical sources for time-tagged data samples, and it overcomes time-bin related drawbacks.

It is a photometric method (e.g., the flux is evaluated within an extraction radius) and, contrary to likelihood based analysis, it lacks the simultaneous study of nearby sources.

It's worth mentioning an other algorithm developed to produce unbinned light curves and show structures within the flare profiles, the Bayesian Block (see Scargle 1998, 2013, and reference therein).

The procedure proposed in this paper is able to resolve candidate flares with a flux (including background) larger than the mean flux and background within the examined period.

In this paper I explain the method following the study case of Fermi-LAT gamma-ray data sample. The generality of the method shows up anyway.

In the following sections, I will present a concise description of the method (section 2), the details of clustering method (section 3 and 4), Scan-Statistics applied to the problem (section 5 and 6), the construction of *unbinned light curves* to identify activity peaks (section 7). All the sections listed above explain the method in the general case of an ordered set of events.

The Monte Carlo study of the procedure and the performance for the Fermi-LAT Telescope will be shown in section 8.

In section 9 I will show examples of application to gamma-ray sources, and I also discuss drawbacks arising with the method.

The proposed method is photometric. The obtained candidate flares could suffer source spatial confusion. The comparison with the full likelihood analysis is mandatory to assess the level of source-confusion, and eventually reject questionable flares.

Section 10 summarizes, performance and weakness of the method for the generic case of ordered data samples.

2. Step-by-step definition of the algorithm

The proposed algorithm is applied to an ordered sample of events of size N .

It consists of: a method of event clustering iterated to obtain all the conceivable clusters from the original sample; an ordering procedure among clusters; and a Statistical evaluation of non-random clusters. The entire method depends on 2 parameters: the statistical Confidence Level (c.l.) and the N_{tol} parameter (its meaning will be explained in section 3, and in appendix A it is explained how to correctly choose it).

Clustering method: The clustering method has two parameters (N_{tol} and Δ_{thr}). The N_{tol} parameter is kept constant. Δ_{thr}

naively corresponds to the maximum allowed distance among the elements belonging to a certain cluster.

The clustering procedure is iterated scanning on the Δ_{thr} parameter. It is finely decreased starting from the largest spacing among contiguous events of the data sample under investigation. The Δ_{thr} decreasing procedure stops when only clusters of size 2 (of two events) remain. At the end of the scanning, the Δ_{thr} space is fully explored.

As far as we can obtain the same cluster from a sub-set of Δ_{thr} , cluster duplicates are removed. No more than N clusters are identified.

For a generic cluster C_i , there are several useful quantities: Cluster size (N_i) is defined as the number of events contained in the cluster. Cluster length (l_i) is the distance from the first to the last event of the cluster. It's also useful to define the effective cluster length $\tilde{l}_i := l_i \cdot (1 + \frac{1}{N_C})$. The event density (ρ_i) is defined as $\rho_i = \frac{N_i-1}{\tilde{l}_i}$. The cluster boundaries are the position of the first and of the last element of the cluster within the extraction interval.

Ordering: I will show that due to cluster definition, the entire set of clusters ($\{C_i\}$) is a single-root tree (as defined in set theory). A set is a single-root tree if an ordering law exists, such that for each element A (except for the root element) of the set, there exists a well-ordered sub-set of elements (the concept of well-ordered set of events is defined in set theory). For the built set of clusters, Δ_{thr} is the order parameter, and the ordering law is the comparison of the order parameter among the clusters.

Within a single-root tree, ancestors/descendant and parent/sons relations are defined. Branches, chains, leaves are defined as well. I will show that the boundaries of a cluster are within the boundaries of other clusters (ancestor/descendant relationship), or the clusters are disjoint. The largest cluster of the set contains all the events. I will denote it *ground cluster*.

In this paper clusters are denoted with C_i , where i is the positional index within the ordered set of clusters. Sometimes the notation C_i^l is used for the same cluster. In this case, the upperscript is the positional index of the parent of C_i .

Removal of random clusters:

It is based on the evaluation of Statistical significance of a son cluster, starting from the null hypothesis that the events of its parent are uniformly distributed.

A multiple window Scan-Statistics based method is used to assess the probability to obtain a cluster by chance starting from the parent cluster.

Once the ordered set $\{C_i\}$ has been prepared, the removal of random clusters is performed starting from ground cluster, and ascending the tree $\{C_i\}$ (e.g., moving in the direction of lowering Δ_{thr}). At first the statistical significance of the ground cluster is evaluated, with the null hypothesis that the events of the whole observing period are uniformly distributed. If the null hypothesis is accepted (according to the chosen confidence level), the ground cluster is removed, otherwise it is maintained within the set of clusters.

For each cluster C_* that has to be evaluated, its parent is identified within the ordered set. The null hypothesis is that the events within the parent cluster are uniformly distributed. If no parent exists within the set of clusters, the null hypothesis is that the events within the whole observing period are uniformly distributed. If the null hypothesis is accepted, then C_* is removed;

otherwise it is kept.

It is a convenient choice to add a special object as first element of $\{C_i\}$. Its boundaries are the start and stop of the whole observing period; its size is the size N of the whole sample; its event density is $\rho_{whole} = \frac{N}{L}$, where L is the duration of the whole observing period. This special object is the *root* of the tree, and it does not obey to the chosen cluster condition.

After removal of random clusters, Two scenarios occur: no clusters remain apart the root (steady source activity), and the root describes the steady case. The opposite case is that some clusters survive the removal procedure. The remaining clusters still form a tree. The leaves of the tree are the activity peaks, and chains connecting the *root* to the leaves describe flaring periods.

The temporal diagram describing the full tree of survived clusters is called *unbinned light-curve*.

3. Clustering Method

A clustering method is applied to an ordered sample of events. The case of Fermi-LAT data is useful to understand, and to apply the procedure:

Suppose We want to study the variability of a gamma-ray source with known coordinates. In this case, the ordered sample is identified with gamma-ray events recorded within a chosen extraction region centered on the source coordinates. The extraction region is chosen according to the instrumental *point spread function* (PSF). As far as the PSF for the event i depends on the reconstructed energy (E_i) and on the morphology of the reconstructed e^-e^+ tracks ($type_i$), I choose the radius of the extraction region coincident with the 68% containment radius at the given energy and the given event type. I denote the extraction region of the event i with $R_{68}(type_i, E_i)$.

The Fermi-LAT exposure to each position of the sky rapidly changes with time, as the satellite scan the whole sky within a few orbit. The cumulative exposure (ξ_i , defined as the exposure from the start of the FERMI-LAT operation to the time of the i^{th} gamma-ray to be scrutinized) is a convenient domain to build the clustering. In facts, for steady sources, the expected number of collected gamma-rays in a time interval is proportional to the exposure of the interval. The time-domain, instead lacks that property.

For each source, The data set is the cumulative exposure ξ_i of the gamma-ray events collected within $R_{68}(type_i, E_i)$ within the chosen observing period.

The data set of the cumulative exposure is denoted with $\{\xi_i\}$, and the ordered set is denoted with $\{\xi_{(i)}\}$. Here, and after in the paper, the generalization of the problem is easily performed, considering the generic ordered set of observables $\{x_{(i)}\}$ (which are supposed to be uniformly distributed) instead of $\{\xi_{(i)}\}$.

Cucala (2008) proposed to define clusters starting from the distance $D_{i,j} = x_{(j)} - x_{(i)}$ for all the ordered events i, j . A different definition of a cluster is the following: Events form a cluster if the relative distance (in the exposure-domain) from each event to the previous one is less than a specified threshold (Δ_{thr}):

$$\xi_{(i)} - \xi_{(i-1)} < \Delta_{thr} . \quad (1)$$

with this definition, a period of steady flux (e.g., for a steady source, or during an activity period with a plateau, such as was reported for 3C 454.3 on the first half of November 2010, see Abdo 2011b) can be fragmented in two or more clusters, due to a peculiar spacing of events: In such a case, when a Δ_{thr}^* is chosen, such that $1/\Delta_{thr}^*$ corresponds to the mean source flux within the period (F_{flat}), the probability for each photon to stay at a distance $> \Delta_{thr}^*$ from the previous one is $1/2$. Hence, the flat flux period corresponds to a large number of clusters (fragmentation, see appendix A for a definition of fragmentation).

To avoid fragments, the definition of a cluster must be changed.

Clusters are defined as the largest uninterrupted sequences of contiguous events of the ordered set $\{\xi_{(i)}\}$, such that for each event l of each sequence, there exist the elements i and $i + k$ of $\{\xi_{(i)}\}$ for which the following conditions are satisfied:

$$\begin{cases} l \in [i, i + k] \\ \xi_{(i+k)} - \xi_{(i)} < k \cdot \Delta_{thr} \quad (k \leq N_{tol}) \end{cases} \quad (2)$$

where N_{tol} is a tolerance parameter for the cluster definition. The clustering scheme reported in eq. 2 is called *short range search* (SRS) clustering scheme². Eq. 2 is forward-backward symmetric: substituting i with $i - k$ we obtain $\xi_{(i)} - \xi_{(i-k)} < k \cdot \Delta_{thr}$ ($k \leq N_{tol}$).

With this cluster definition, both elements i and $i + k$ (or $i - k$) are elements of the same cluster. Moreover all the elements between i and $i + k$ (or $i - k$) are elements of the same cluster.

If $N_{tol} = 1$ the cluster definition of eq. 2 corresponds to the definition in eq. 1. The cluster definition of eq. 2 simply states that on average the distance among elements of a cluster must be $\leq \Delta_{thr}$. N_{tol} is the maximum allowed number of elements for which the average distance can be evaluated.

This generalization of the definition of clusters largely reduces fragmentation of periods of flat flux.

The cluster definition of eq. 2 searches for clusters starting from contiguous events, and two contiguous flares (F_a and F_b) are glued together when the first event of F_B and the last event of F_A obey eq. 2. It is necessary for gluing that there are no more than $2 \cdot N_{tol}$ events in-between the two flares. The proposed procedure does not try to merge distant flares, with the cost of introducing the N_{tol} parameter. Instead, the method proposed in Cucala (2008) try to merge distant flares. In appendix B I will discuss the gluing effect.

4. The iterated clustering procedure (iSRS)

For a given ordered data-set, events can be clustered choosing Δ_{thr} , and N_{tol} . For an extremely high Δ_{thr} (larger than the maximum spacing between two contiguous events Δ^{max}) the ground cluster C_0 is identified. It contains all the events of the data-set. A fine Scan is performed varying the value of Δ_{thr} (but for a fixed value of N_{tol}): starting with $\Delta_{thr} = \Delta^{max}$; the scan stops when only clusters of size 2 (of two events) remain.

No particular attention is paid to decide the step of the scan. It has been chosen an exponentially decreasing step, 20 steps per decade. The fine-scan on Δ_{thr} is called here *iterated SRS* (iSRS)

² The C language code to identify clusters according to eq. 2 is available in electronic form at the CDS via anonymous ftp to cdsarc.u-strasbg.fr (130.79.128.5) or via <http://cdsweb.u-strasbg.fr/cgi-bin/qcat?J/A+A/>

clustering³.

Lowering the threshold (e.g., the allowed distance among elements of the cluster), smaller clusters (with respect to C_0) can be obtained. The event density of each new cluster is higher than the event density of C_0 , because the average distance among contiguous elements of each new cluster is lower.

Keeping constant N_{tol} , each cluster is characterized by Δ_{thr} , the cluster length, cluster size, and position within the originating segment.

With the iSRS clustering, all the clusters of m events can be found ($\forall m \in (2, N]$). We obtain a set $\{C_i\}$ of clusters ordered by the value of Δ_{thr} .

It could happen that the same cluster is obtained for different values of Δ_{thr} . Only one among identical clusters is maintained.

The set $\{C_i\}$ can be organized as a single-root tree of decreasing size (of events) and decreasing length: Suppose a cluster C_A is formed for a given Δ_{thr}^A . Decreasing Δ_{thr} , we cannot obtain a cluster including events within C_A and events outside C_A . In fact, to obtain this sort of cluster at a Δ_{thr}' , there must exist at least an event outside C_A and an event within C_A that satisfy the cluster condition of eq. 2. But, this condition is never satisfied at Δ_{thr}^A , thence it cannot be satisfied at Δ_{thr}' , because $\Delta_{thr}' < \Delta_{thr}^A$.

On the contrary, decreasing the threshold below Δ_{thr}^A , events within C_A can form shorter clusters, because the condition of eq. 2 could be only satisfied for a sub-set of the events of C_A . More in general, the intersection of two clusters C_A and C_B coincides with the smallest one or it is the Empty Set. in the case $C_A \cap C_B \neq \emptyset$, the Δ_{thr} parameter is an order parameter among the two clusters:

$$\left\{ \begin{array}{ll} C_A \cap C_B = \emptyset & \\ \text{or} & \\ C_A \subset C_B & \text{if } \Delta_{thr}^A > \Delta_{thr}^B \\ \text{or} & \\ C_A \supset C_B & \text{if } \Delta_{thr}^A < \Delta_{thr}^B. \end{array} \right. \quad (3)$$

where Δ_{thr}^A and Δ_{thr}^B are the threshold used to form clusters A and B respectively.

These are the only conditions needed to build a single-root tree structure: The whole set of clusters obtained scanning on Δ_{thr} are nodes of a tree.

Starting from C_0 and ascending the tree (e.g., going in the direction of lowering Δ_{thr}) the formed clusters are characterized by decreasing number of events, and by the property that the boundaries of a cluster C_j is contained within the boundaries of other clusters (*ancestor* clusters).

We can identify an ancestor/descendant hierarchy: Starting from a cluster C_A , it can be identified as an ancestor if there exists at least an other cluster C_B such that:

$$C_A \subset C_B. \quad (4)$$

If such a condition is satisfied, C_B is a descendant of C_A ; otherwise C_A is a leaf of the tree.

C_0 is the ancestor of all the other clusters.

Due to eq. 3, the total number of built clusters is $\leq N$.

³ The C language code performing the iSRS clustering is available in electronic form at the CDS via anonymous ftp to cdsarc.u-strasbg.fr (130.79.128.5) or via <http://cdsweb.u-strasbg.fr/cgi-bin/qcat?J/A+A/>

5. Coincidence Cluster Probability

There is a chance that reconstructed clusters does not represent a flaring period, but a statistical fluctuation over the true flux of the source. To estimate the probability of obtaining a cluster by chance, I consider as null hypothesis, the case that the whole sample is uniformly distributed within the extraction interval (for the Fermi-LAT data sample the case that the background diffuse emission, background sources and the foreground source give a steady contribution during the observing period within the extraction region $R_{68}(type_i, E_i)$).

Suppose we have N uniformly distributed events within the extraction interval. For the case of the Fermi-LAT data sample the extraction interval is the cumulative exposure domain (it has not to be confused with the extraction region in aperture photometry); let us assume without loss of generality that the extraction interval is the unitary extraction interval $(0, 1]$. Suppose we count the events within a window of fixed length (d) within the extraction length. Suppose also that the window is moved within the unitary extraction interval. Following the notation in Glaz (1994), scan-statistics evaluates the probability $P\{N_d > m\}$ to found more than m events within a moving window of length d (with d contained in the unitary extraction length), where: $N_d = \sup\{N_{x,x+d}; 0 \leq x < 1 - d\}$, $N_{x,x+d}$ is the number of events in the interval $(x, x + d]$, $0 \leq d < 1$ (see Glaz 1994, for a detailed explanation).

In spite of the ease of the enunciation, statisticians took over 30 years to found a solution for $P\{N_d > m\}$ (Huntington & Naus 1975). The implementation of the solution is practically unfeasible and approximate solutions are often proposed (see, e.g., Huffer & Lin 1997; Haiman & Preda 2009).

To approach the problem I made use of the relation reported in Glaz (1994):

$$P\{N_d > m\} = P\{S_{(1)}^{(m)}\} \quad (5)$$

where $P\{S_{(1)}^{(m)}\}$ is the distribution of the smallest of the m-spacings. The m-spacings S_i^m are defined by:

$$S_i^m = X_{(m+i)} - X_{(i)} \quad (6)$$

where $\{X_{(i)}\}$ is the ordered set of uniformly distributed events $\{X_i\}$, and $\{S_{(i)}^{(m)}\}$ is the ordered set of m-spacings $\{S_i^{(m)}\}$ (see Glaz 1994, and references thereafter for detailed definitions).

The distribution of $S_{(1)}^{(m)}$ can be easily obtained with simulations.

Tables were prepared with the cumulative distribution of $S_{(1)}^{(m)}$ for a uniform distribution of N points on a segment. Tables cover values of N from 3 up to 10^6 .

Tables are filled up running $N_R = 4 \times 10^6$ random samples of N events extracted with a uniform distribution.

The number of total random extractions is of the order of 10^{15} to fill all the tables. I used the Marsaglia-Zaman RANMAR random engine (Marsaglia 1990; James 1990) contained in the CLHEP library which has a very long recycling-period $\sim 10^{144}$, and does not show correlated sequences of extracted variables (nearby generated points are not mapped into other sequences of nearby points).

Each table corresponds to a fixed sample size N^* . Each row of a table contains the distribution for a fixed m-spacing. Each element of a row reports the length $S_{(1)}^{(m)}$ of the m-spacing which corresponds to a certain probability $P^*\{S_{(1)}^{(m)}\}$. Columns are prepared for probabilities $P^* = \frac{1}{\sqrt{2\pi}} \int_t^\infty e^{-\frac{t^2}{2}} dt$ with $t=2$,

2.5, 3, 3.5, 4, 4.5. The reported lengths of m-spacings have a statistical accuracy which corresponds to a relative accuracy on probability $\frac{\Delta P^*}{P^*}$ of 0.3%, 0.6%, 1.3%, 3.3%, 8.8%, 27% for $t=2, 2.5, 3, 3.5, 4, 4.5$ respectively. For $N \leq 300$, the tables for all the m-spacings and for all the sample sizes were filled.

Scan-statistics cannot be applied directly to search for flaring period, because it makes use of a moving-window of fixed length (d in the discussion above). The analyst must know the duration of the flare in advance, to choose the value of d . Nagarwalla (1996); Glaz & Zhang (2006); Cucala (2008) investigated the problem. In particular Glaz & Zhang (2006); Cucala (2008) applied scan-statistics approach iterated on a set of windows of different length.

Once a set $\{C_i\}$ of clusters is obtained, we want to investigate if they could be considered or not random fluctuations from an uniform distribution extracted within the extraction interval.

If the problem is limited to study the subsample of $\{C_i\}$ which consists only of clusters of fixed size, the problem is univariate, and the m-spacing statistics can be applied directly (using eq. 5 and the tables with the distribution of $S_{(1)}^{(m)}$) to evaluate chance cluster probability which is called here $P_{scan}(C_i)$ to underline that it is valid for the scan-statistic case). But the case we have to face with is that the cluster size is not held fixed: the distribution of $\{C_i\}$ is multivariate, and $P_{scan}(C_i)$ does not correspond to chance cluster probability.

Anyway, we can report $P_{scan}(C_i)$ in Gaussian standard deviation units t_{scan}^i , where the info of C_i are all contained in the index i . From every C_i we evaluate t_{scan}^i . From the entire set $\{C_i\}$ we obtain the set $\{t_{scan}^i\}$. We study the statistical distribution of

$$\Theta = \max\{t_{scan}^i\} \quad (7)$$

where the maximum is evaluated over all the formed clusters. Θ is called *Maximum Scan Score Statistic* (Glaz & Zhang 2006). Θ has an univariate distribution that can be studied with simulations in the case of an uniform data-set:

For every simulated sample of size N , We apply the iSRS clustering procedure, and we obtain $\{C_i\}$ (and thence $\{t_{scan}^i\}$). From $\{t_{scan}^i\}$, we found Θ according to eq. 7.

From a set of simulated samples (with the same size N), the distribution of Θ is obtained.

We define *false-positive* a sample with Θ above a predefined value Θ^* . f_{coinc} is the frequency of false-positive samples. It can be denoted with $f_{coinc}(\Theta^*)$. The cumulative distribution of Θ is $1 - f_{coinc}(\Theta^*)$.

The Monte Carlo results are reported in figure 1: I show the obtained f_{coinc} as a function of sample size N , for a set of chosen Θ^* .

The curves reported in figure 1 shows a change of slope for sample-sizes below ~ 30 . It is neither due to approximations on the distribution of $S_{(1)}^{(m)}$, nor to the interpolations for the m-spacings and for the sample-sizes, because, for sample-sizes below ~ 300 , the tables for all the m-spacings and for all the sample sizes were filled.

The m-spacings tables were used to evaluate f_{coinc} . If a table for a given sample-size has not been prepared, an interpolation using the tables with the nearest sample-sizes is performed. If a m-spacing row for a certain sample size has not been prepared, an interpolation using the nearest m-spacings is performed. The systematic on false-positive frequency is due to the accuracy of

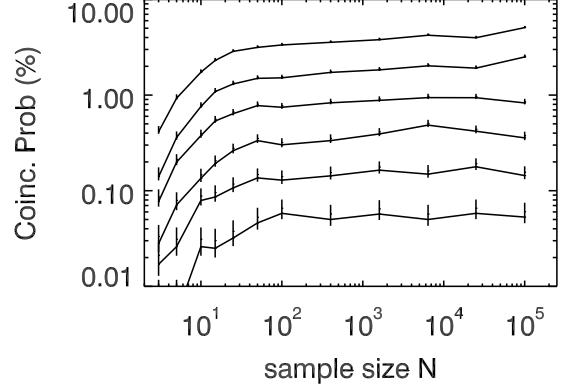


Fig. 1. Cluster Coincidence Probability prepared with a Monte Carlo for samples of N events. Curves refer to the frequency of false-positive samples obtained for different Θ^* thresholds: from top to bottom $\Theta^* = 2.75, 3, 3.25, 3.5, 3.75, 4$.

the m-spacings tables, and on the interpolations on sample-size and on m-spacing. Statistical accuracy of m-spacing tables has been already discussed. Interpolation on sample size was found to introduce a systematic relative error of 10% on the evaluation of f_{coinc} . The interpolation on m-spacings introduces a systematic relative error of 7%, 2%, $< 1\%$ for sample of size $10^5, 25000, 1600$ respectively.

In the following, I refer to the probability distribution of Θ with $P_{iSRS}(t_{iSRS})$ in standard Gaussian units) to underline that it is obtained without constraints on the cluster-size, and using the iSRS clustering scheme.

6. Removal of random Clusters

We have prepared a set $\{C_i\}$ from the original sample using the iSRS clustering. If the source was steady, the distribution of Θ prepared applying eq. 7 to the set $\{C_i\}$ is known. We can choose a confidence level, and find the corresponding Θ_{cl} : If we have an uniformly distributed sample of size N , there is a probability coincident with the confidence level that:

$$\Theta < \Theta_{cl} \quad (8)$$

If the source, instead, had a flare, the m-spacings are not distributed as in the case of an uniformly distributed sample. As a consequence, Θ also is not distributed as in the case of an uniformly distributed sample, and for a sub-set of clusters $\{\tilde{C}_i\}$, we could obtain values of $t_{scan}^i > \Theta_{cl}$. I will use eq. 8 to test the hypothesis that the sample under investigation is uniformly distributed, and I call *statistically relevant* with respect to the whole investigated period the clusters of the sub-sample $\{\tilde{C}_i\}$.

For a reason that will become obvious in a while, a special object is added as first element of $\{C_i\}$. Its boundaries are the start and stop of the observation; Its effective length (\tilde{l}_{whole}) is the whole extraction interval, and its size (N_{whole}) is the sample size N . I will denote it with C_{whole} . It does not obey eq. 2. It is the *root*.

The set $\{C_i\}$ is ordered with respect to Δ_{thr} . The clusters of the ordered set $\{C_i\}$ have to be considered as candidates. A discrimination procedure is applied in order to build a

sub-set of clusters that describe the source variability within the investigated period:

The removal procedure is applied to all the clusters starting from C_0 , and continuing with the clusters with lower Δ_{thr} . At first step, we have to evaluate if C_0 has to be considered as a random fluctuation from a uniformly distributed sample of size N and extracted within the whole period of investigation. If C_0 belongs to the sub-set of statistically relevant clusters it is maintained, otherwise it is removed from the original set.

If C_0 is maintained, the most conservative hypothesis is that the events within C_0 are uniformly extracted within a period of length coincident with the effective length of C_0 .

Going on with the removal procedure, for a certain index of the ordered list of candidate clusters, we found a cluster C_* . We have to choose if accept or reject C_* : We identify uniquely its direct accepted ancestor C_p (parent). Due to the fact that the removal procedure is ordered with respect to Δ_{thr} , C_p has already been accepted. The most conservative hypothesis (null hypothesis) is that the sample (of size N_p) of the events contained in C_p is uniformly distributed within the effective length (\tilde{l}_p) of C_p (e.g., that the source flux was steady during the period identified with C_p). If no parent cluster exists, the root (C_{whole}) is considered as parent instead, and N_{whole} and \tilde{l}_{whole} are used. We accept C_* if the null hypothesis is rejected according to the chosen confidence level. The removal decision of cluster C_* follows the same arguments used for the removal decision of cluster C_0 , but instead of evaluating if C_* is a statistically relevant cluster with respect to the whole investigated period, we make the following evaluation: We restrict to the reduced sample of events contained in C_p . This sample is of size N_p , and it is assumed to be of length \tilde{l}_p . We evaluate if C_* is among the statistically relevant clusters for the reduced sample. I call these clusters *statistically relevant with respect to the period described by the cluster C_p* , or, more concisely: *statistically relevant with respect to C_p* . If C_* is statistically relevant with respect to C_p , it is maintained, otherwise it is removed. If C_* is maintained, the new conservative hypothesis is that C_* describes a period of steady activity.

The statistical discrimination procedure is performed for all of the candidate clusters. The flowchart of the procedure is reported in fig. 2.

The surviving clusters have new properties:

1. They are all statistically relevant with respect to their own parents ;
2. The events contained in any parent cluster do not belong to an uniform distribution .

7. Unbinned light curves

Two opposite scenarios are discussed: a steady, and a flaring source.

If the source was steady during the whole observing period, we expect no cluster to survive the removal of random clusters, apart the root C_{whole} .

There is a chance probability $<1.3\%$ (if the confidence level is set to 99.87%) to obtain one or more clusters from a uniformly distributed sample.

It is useful to walk again through the iterated SRS clustering, and through the removal of random clusters for the case of a source that underwent a flare during the investigated period. The cluster property 2 states that clusters, and chains of clusters are

expected during activity periods (when the hypothesis of steady source is false):

Once the set $\{C_i\}$ is prepared, there could be at least a candidate son cluster $C_i^{whole}(\xi_{thr_i})$ which is statistically relevant with respect to the whole observing period (if there are several relevant clusters, the one with the largest Δ_{thr} is chosen). In this case, the null hypothesis of a steady source is rejected, and the new conservative hypothesis is that C_i^{whole} corresponds to a period of flat activity.

Continuing the removal of random cluster procedure, we could find at least a cluster C_j^i (descendant of an accepted cluster C_i) which is statistically relevant with respect to the period identified with C_i (if there are several relevant clusters, the one with the largest Δ_{thr} is chosen). We reject the hypothesis of a steady source within the period identified with C_i , and maintain the cluster C_j^i . The new conservative hypothesis is that the cluster C_j^i identifies a period of flat activity.

The procedure stops when no son clusters exist for which the new conservative hypothesis can be statistically rejected.

Clusters with no sons identify the flare peaks: the leaves of the tree are found when the flare peak is found (the light-curve at its peak is locally flat), or the paucity of collected photons prevents the procedure to go on). The set $C_i^{whole}, C_j^i, C_k^j, \dots, C_m^l, C_n^m$ is the chain describing the flaring period. C_n^m is a leaf of the tree. It represents the activity peak.

Property 1 states that each cluster of the chain is statistically relevant with respect to its parent: the chain of clusters is a statistically filtered representation of the flaring period. Examples of real unbinned light curves are reported in fig. 7 and 8. Each horizontal segment represents a cluster of the tree: it subtends the temporal interval characterizing the cluster; its length is the effective length of the cluster in the temporal domain; its height is the mean photometric flux of the source within the subtended temporal interval.

Each reported cluster cannot be considered a random fluctuation (according to the chosen C.L.) from a flat activity period identified by its parent cluster.

The unbinned light curve as a whole is a representation of the tree like hierarchy. The peaks of flare activity are the clusters with no associated sons. This means that within each identified period of activity peak, we did not found any statistically relevant sub-set of events describing a period of larger flux. The identification of the activity peaks is a direct result of the unbinned light curve procedure.

The reported clusters are not independent. Eq. 3 and 4 state that clusters describing the same flare are all correlated, because their intersection is not the empty set. Thence, the evaluation of the temporal FWHM of reconstructed flares can be performed starting from the unbinned light curve, but the statistical uncertainty of the temporal FWHM must be evaluated using simulations.

8. Performance of the method for the FERMI-LAT: flare detection efficiency, flare reconstruction capability

I tested the proposed procedure with simulations. As far as gamma-ray background varies with celestial coordinates, and chance detection probability depends on source mean flux and background, the performance of the method depends on the investigated source. I focus here to the case of the Flat Spectrum Radio Quasar 3C 454.3 .

The extraction region is centered on the coordinates of the source, and its radius corresponds to the containment of 68% of photons from the source. Background level corresponds to the observed background for the source (In appendix D I will show the method to evaluate background). I computed the FERMI-LAT exposure for 3C 454.3 with a binsize of 86.4 s from the beginning of FERMI-LAT scientific operations, till 2015-11-16 (see appendix C for the details of exposure preparation).

I simulated ideal flares photon by photon with a temporal shape

$$F(t) = A \left(1 - e^{-\frac{t-t_0}{\tau_1}} \right) e^{-\frac{t-t_0}{\tau_2}}. \quad (9)$$

In order to reduce the total number of simulation runs, I chose $\tau_1 = \tau_2 = \tau$. Coefficients A and τ are chosen to simulate flares with a given peak flux and temporal *FWHM*.

Ideal flares are simulated assuming a flat exposure. I used the computed exposure to accept or reject simulated photons from the source and from background. The accepted photons are the final photon list.

The chosen threshold probability P_{iRS}^{thr} is 99.87% (e.g., $t_{iRS}^{thr} = 3$).

In figure 3 I report the detection efficiency for flares with a temporal *FWHM* of 0.01, 0.1, 1, 10, 100 d, and with peak flux from 10^{-8} to 10^{-5} ph cm $^{-2}$ s $^{-1}$ ($E > 0.3$ GeV). For flares with a *FWHM* above 1 d (slow flares), the detection efficiency rises fast around the threshold flux. On the contrary, below 1d (fast flares), it rises slowly, because the FERMI-LAT observes sources for windows of 10-20 minutes each orbit or two (and sometime 4). Extremely fast and bright flares can be detected, even if their peak emission lies outside the observing windows, provided that the sampled tails of that flares are bright enough to be detected. The flux $F_{50\%}$ ($F_{20\%}$) corresponding to a detection efficiency of 50% (20%) is reported in figure 4 as a function of temporal *FWHM* of the simulated flares. Two cases are reported, corresponding to faint ($N^{SRC} \leq 0.2N^{BKG}$) and bright sources ($N^{SRC} \sim 16N^{BKG}$), where N^{SRC} and N^{BKG} correspond to the total source and background counts integrated in 7.25 years with Fermi-LAT collected in the chosen extraction region. Below 0.01 d, the computed values of $F_{20\%}$ is very similar for bright and faint sources, because flares could be detected, provided they happen outside the exposure gaps: the satellite pointing strategy affects the detection efficiency and dominates over statistic.

The peak flux reconstruction capability is reported in figure 5. For bright flares the Reconstructed flux (F_{rec}) approaches F_{peak} . In the region where the detection efficiency (see fig. 3) is larger than $\sim \frac{1}{2}$, the Reconstructed flux (F_{rec}) is in the range $F_{peak}/2 < F_{rec} \leq F_{peak}$. The ratio F_{rec}/F_{peak} increases while F_{peak} increases. For the brightest flares F_{rec} approaches F_{peak} . The lowering of F_{rec}/F_{peak} for faint flares is due to the fact that for faint flares, the activity peak is not well resolved.

In the region where the detection efficiency is smaller than $\frac{1}{2}$, the ratio F_{rec}/F_{peak} increases while the F_{peak} decreases, and it is lower than 2.

For flares shorter than 1 d, the reconstructed flux shows large deviations from the simulated one, because of the FERMI-LAT observing strategy (for the majority of the flares the peak flux is not sampled at all). For flares of *FWHM*=0.01 d, on average the ratio F_{rec}/F_{peak} decreases while F_{peak} increases. The reason is that faint flares are preferentially detected when the peak of emission is sampled.

Temporal *FWHM* is estimated starting from the unbinned light curves. It is derived assuming that the underlying flare has a pyramidal shape. The temporal *FWHM* reconstruction capability is reported in fig. 6. For flares with temporal *FWHM* larger than 1 d, the reconstruction capability is poor for faint flares, and the reconstructed *FWHM* exceed the simulated *FWHM*. The *FWHM* of flares with simulated *FWHM* shorter than 1 d cannot be reconstructed, due to the temporal gaps of the exposure.

9. Results for some gamma-ray samples and Conclusion

Extensive results for an astrophysical problem will be shown in a forthcoming paper. To explain advantages and drawbacks of the method, I report here some case (Details about data-preparations are in appendix C.

McConville (2011) studied the activity of the Flat Spectrum Radio Quasar 4C +55.17 from 2008 August to 2010 March. They found no evidence for gamma-ray variability within the scrutinized period. The authors also found energy emission up to 145 GeV (observer frame). Their multiwavelength investigation shows the source is compatible with a young radio source, with weak or absent variability.

The unbinned photometric light curve of the source for a period of 7.25 years of monitoring in gamma-ray does not show flaring activity in the range 0.3-500 GeV with a confidence level of 99.87%.

I show here the unbinned photometric light curves for the Crab Nebula in the energy range 0.1-500 GeV (fig. 7), and for the Flat Spectrum Radio Quasar 3C 454.3 (fig. 8) in the energy range 0.3-500 GeV.

These sources are among the brightest gamma-ray sources in the sky, and the unbinned light curves are fully representative of source variability.

For both the sources I used $N_{tot} = 50$ to reduce fragmentation. In figures 7 and 8 background is not subtracted, but it is negligible. Each horizontal line represents the mean source flux (including background sources and diffuse background emission). The ground level is the mean source flux (+background) over the whole scrutinized period. Each horizontal segment is statistically relevant above the father one according to the chosen confidence level.

The Crab large variability in gamma-ray was first observed with AGILE (Pittori 2009; Tavani 2011). They argue the variability is due to a component with a cutoff around 0.5 GeV, so I report here the unbinned light curve obtained for confidence levels of 99.87%, in the energy range 0.1 - 500 GeV. In the low energy band the instrumental PSF of the FERMI-LAT is large, but the Crab flux is extremely bright and contamination from nearby sources can be neglected. The unbinned photometric light curves reported here refer to the FERMI-LAT observing period only.

Due to the complex unbinned light curve of the Crab Nebula, I report in figure 7 two periods only, referring to: the flaring period investigated in Striani (2013) and in Abdo (2011a) (panel a); and the one investigated in Buehler (2012) (panel b). The comparison among the unbinned light curve proposed here and previous works is useful to show the power and weakness of the proposed method. The top panel in figure 7 shows a flare that is not well resolved in Abdo (2011a). The same flare is reported also as F7 in Striani (2013). I obtain a peak photometric flux

on MJD 55459.793. The temporal FWHM estimated from the unbinned light curve reported here is 0.23 ± 0.12 d (the error is evaluated from the Monte Carlo simulations reported in fig. 6). The temporal FWHM could be overestimated by a factor ~ 2 . The unbinned light curve analysis shows that it is the shortest flare ever reported for the source so far.

The feature F6 in Striani (2013) is not detected with the unbinned light curve, but in the approach proposed here, clusters with low statistical significance are disregarded.

The other panel in figure 7 can be compared to finely segmented light curve produced with likelihood analysis in Buehler (2012). That authors prepared a fixed exposure light curves (the binning is variable in time, the mean bin duration is 9'). The analysis in Buehler (2012) makes use of the Bayesian Block procedure for binned data to statistically evaluate variability, and performs an exponential fitting of the rising part of the two resolved flares.

The method proposed in this paper reveals the same two flares, centered on MJD 55665.110 and MJD 55667.319, with temporal FWHM of 1.2 ± 0.4 d and 1.1 ± 0.4 d respectively, in agreement with the results reported in Buehler (2012).

Flares from the FSRQ 3C 454.3 are intensively studied. The binned light curve for the first 3 years of FERMI-LAT observations of 3C 454.3 is reported in Abdo (2011b) with a time bin of 1 day. The light curve for the first 5.1 years of FERMI-LAT observations is reported in Pacciani (2014) with a time-bin of 4 days ($E > 0.3$ GeV). The light curve for the following 1 year of the source is reported in Britto (2016) with 1 day time bin. A shorter period of activity is reported with 3hr time bin in Coogan (2016) and in Britto (2016). The procedure proposed here detects the flares of the source with some exception: It does not detect the secondary flare around MJD 55330 shown in the 0.1-500 GeV light curve reported in Abdo (2011b). It is detected integrating data in the 0.1-500 GeV with a confidence level of 99.87%.

In Abdo (2011b), authors report a flare fine-structure during the brightest activity period of the source (around MJD 55517 - 55520), and they investigated the fine-structure fitting a model of 4 flares to the data in the 0.1-500 GeV energy range. The method proposed here reveals a single flare in the energy range 0.3 - 500 GeV (with 99.87% c.l.), without making assumptions on flare shape. Substructures emerge integrating data in the 0.1-500 GeV (97.7% c.l.). In conclusion, for the brightest flares, the study of fine-structure making use of a fitting strategy, is the preferred method, that has to be statistically compared with the null hypothesis of a single flare.

The unbinned photometric light curves shown here for the Crab Nebula (fig. 7) and for the FSRQ 3C 454.3 (fig. 8) show both the advantage of the procedure, both the remaining drawbacks:

Peak flux activity period is resolved only when it is larger than the mean flux (including diffuse background and nearby sources). Weak flares from faint sources, surrounded by bright sources, cannot be resolved. This is the case of 3C 345, whose flaring activity (see, e.g., Reyes 2009) is washed out by the presence of the nearby bright sources 4C 38.41, Mkn 501 and NRAO 512 at 2.2° , 2.1° , and 0.48° from the foreground source respectively.

Isolated flares are resolved according to sensitivity limit.

As far as there is no time-binning, there are no time-bin related

issue. The detection of fast flares from the Crab Nebula, and large temporal structures as in the case of 3C 454.3 is obtained without ad-hoc assumptions, or peculiar choices in the analysis. There is however a resolving-power drawback. In fact there is the need to define N_{tol} to avoid fragmentation. The consequence is that consecutive flares, whose peak activity are separated by less than $2N_{tol}$ gamma-rays could be merged together, as discussed in appendix B; merging involves faint flares.

A fraction of fast and bright flares can be detected depending on the pointing strategy of the FERMI satellite. I evaluated that FERMI-LAT can detect flares with a temporal FWHM as short as 10-20 minutes and peak flux $\sim 10^{-5}$ ph cm $^{-2}$ s $^{-1}$ ($E > 0.3$ GeV) with a detection efficiency of 20% (at 99.87% c.l.). But this evaluation depends on the temporal profile of the flare. It is difficult, indeed, to evaluate peak flux and temporal FWHM of bright flares with typical timescale less than 0.1-0.3 d.

10. Discussion

I have developed a procedure to identify activity peaks in time-tagged data. I applied the proposed procedure to gamma-ray data only, but it can be applied to any time-tagged data-set, or more in general to any ordered set of uniformly distributed events.

The basic task of the procedure is the identification of statistically relevant periods within a supposed uniformly distributed sample. There are no fitting in the procedure, thence no fitting-related convergence issue. I have shown with simulations and with real data, that the procedure is capable to detect activity peaks without any prior knowledge of their shape and temporal size.

There is a parameter in the procedure (N_{tol}) introduced to face with fragmentation artifact. I have shown how to choose it, and the drawback arising with its introduction. Small samples (of 10^3 events or less) can be statistically investigated to search for variability and N_{tol} could be safely set to 1 for these samples.

The knowledge of performance and limitation of a method are crucial to apply it to any Astrophysical case. I explored the limitation of the procedure. I also investigated sensitivity limit and performance of the method for a specific case.

The procedure is based on scan-statistics, and on extensive Monte Carlo simulations. Results of simulations are for a general use, and are contained in short tables for the statistics of m-spacings and for the frequency of false-positive samples.

Even if it is conceivable to extend tables to extremely large samples, the introduction of asymptotic scaling laws could be appropriate to overcome large computational effort. A step toward this direction is performed in Prah (1999). The author developed a Poisson test based on a semi-analytical method. The test is based on the distance among contiguous events (e.g. on the m-spacing problem, with $m = 1$). The extension of that semi-analytical method to $m > 1$ is indeed mandatory to explore the full spectrum of variability for extremely large samples. Other approaches to obtain asymptotic solutions to the problem are investigated, e.g., in Huffer (1997) and in Boutsikas (2009).

The computational effort to produce unbinned light curves from an ordered set of N events is extremely low (once the chance cluster probabilities are all tabulated): The procedure that produces clusters evaluates no more than $N_{tol} \cdot N$ distances among

events. For all the examples reported, the iteration on Δ_{thr} spans no more than 5 decades with 20 steps per decade. The total number of evaluated distances is thence no more than $100 \cdot N_{tol} \cdot N$. The total number of clusters is no more than N , because the intersection of two clusters coincides with the smallest of them or it is the Empty Set.

As far as chance cluster probabilities are all tabulated, no more than N probabilities are extracted from the tables.

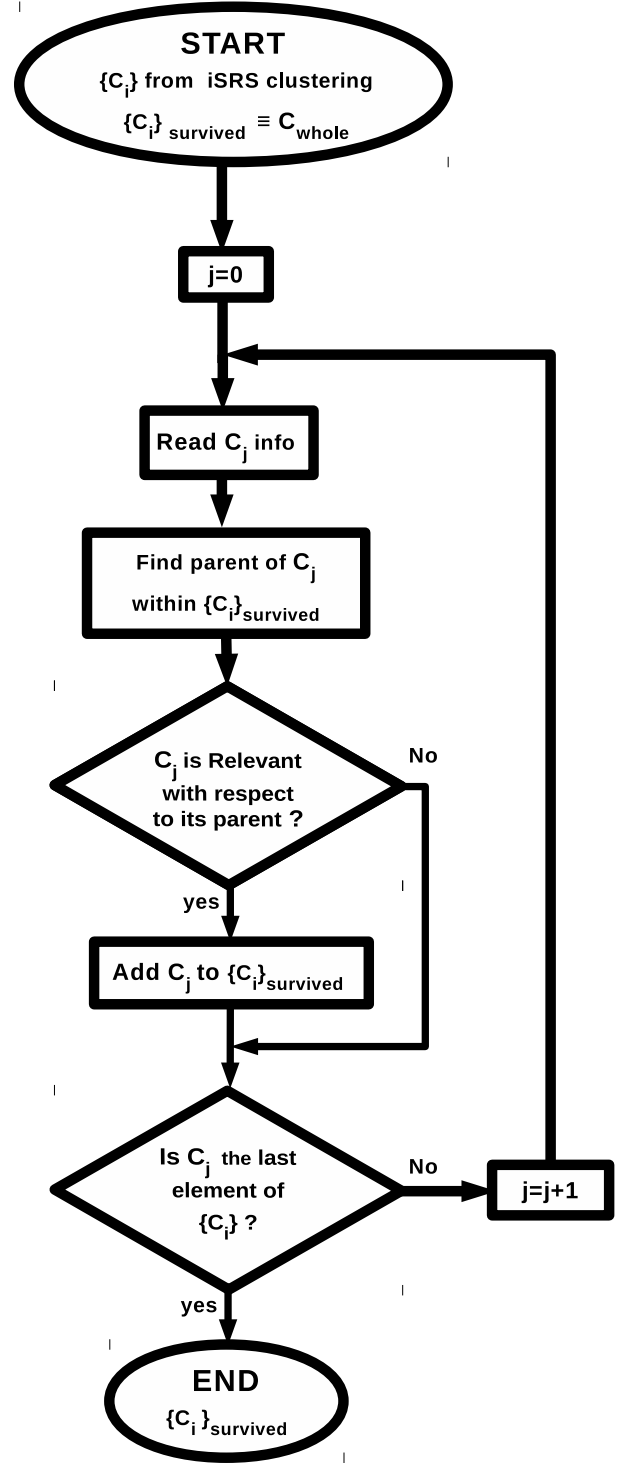


Fig. 2. Flowchart of the removal of random clusters. At beginning we have the ordered set $\{C_i\}$ obtained with the iSRS clustering. The initial list of survived clusters $\{C_i\}_{survived}$ contains only the special cluster C_{whole} . At step j , cluster C_j of the ordered set $\{C_i\}$ is evaluated: its parent is identified within the current list $\{C_i\}_{survived}$ (if no parent cluster exists, C_{whole} is used as parent). If the cluster C_j is among the statistically relevant clusters with respect to its parent, it is added to $\{C_i\}_{survived}$. When all the cluster of the initial set $\{C_i\}$ are evaluated, the procedure stops and $\{C_i\}_{survived}$ is built.

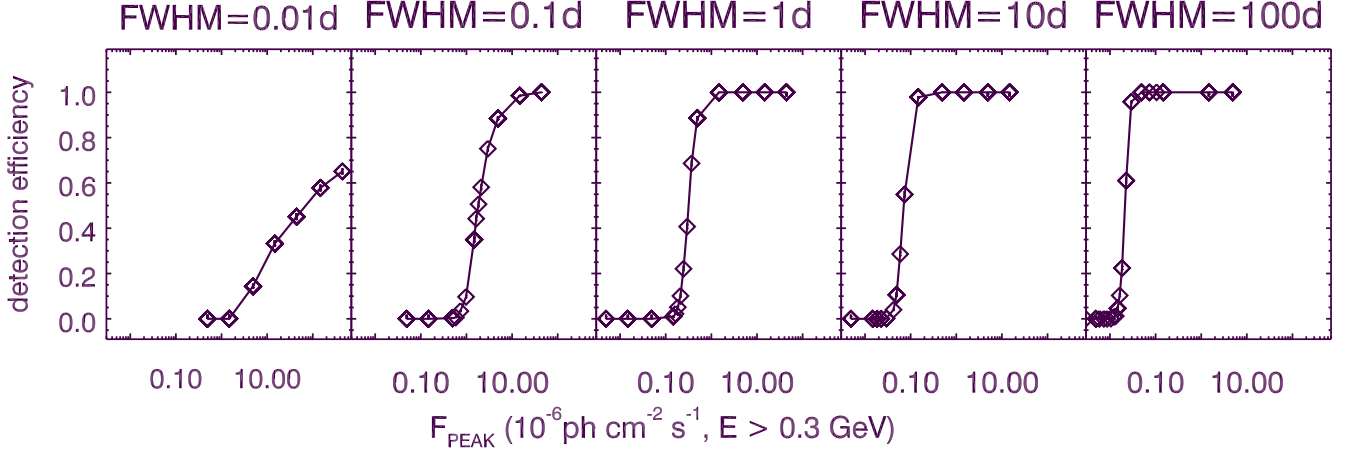


Fig. 3. Detection efficiency for flares with FWHM of 0.01, 0.1, 1, 10, 100 d as a function of the simulated flare peak flux. The observing period is 7.25 y.

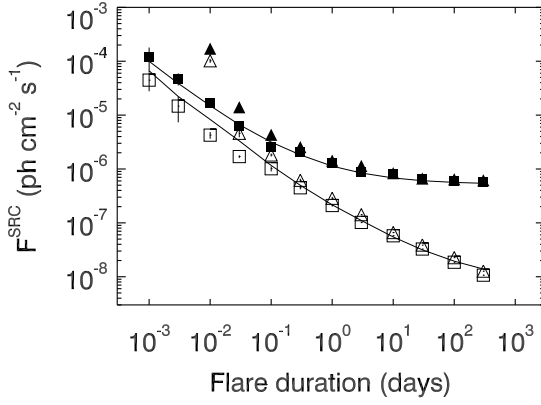


Fig. 4. Peak flux detection threshold as a function of the simulated flare duration, reported as FWHM. Triangles (squares): Flux threshold is defined as the peak flux for which half (20%) of the simulated flares are detected. The observing period is 7.25 y, $E > 0.3$ GeV, The extraction radius corresponds to the containment radius for the 68% of events. Open squares and triangles refers to a faint source (giving a total number of counts on FERMI-LAT which is 20% of the background counts within the scrutinized period). Filled symbols refer to a bright source (corresponding to the case of 3C 454.3). Curves refer to sensitivities calculated assuming constant exposure, hat shaped flares, for $t_{IRS}^{thr} = 3$. (e.g., 99.87% c.l.).

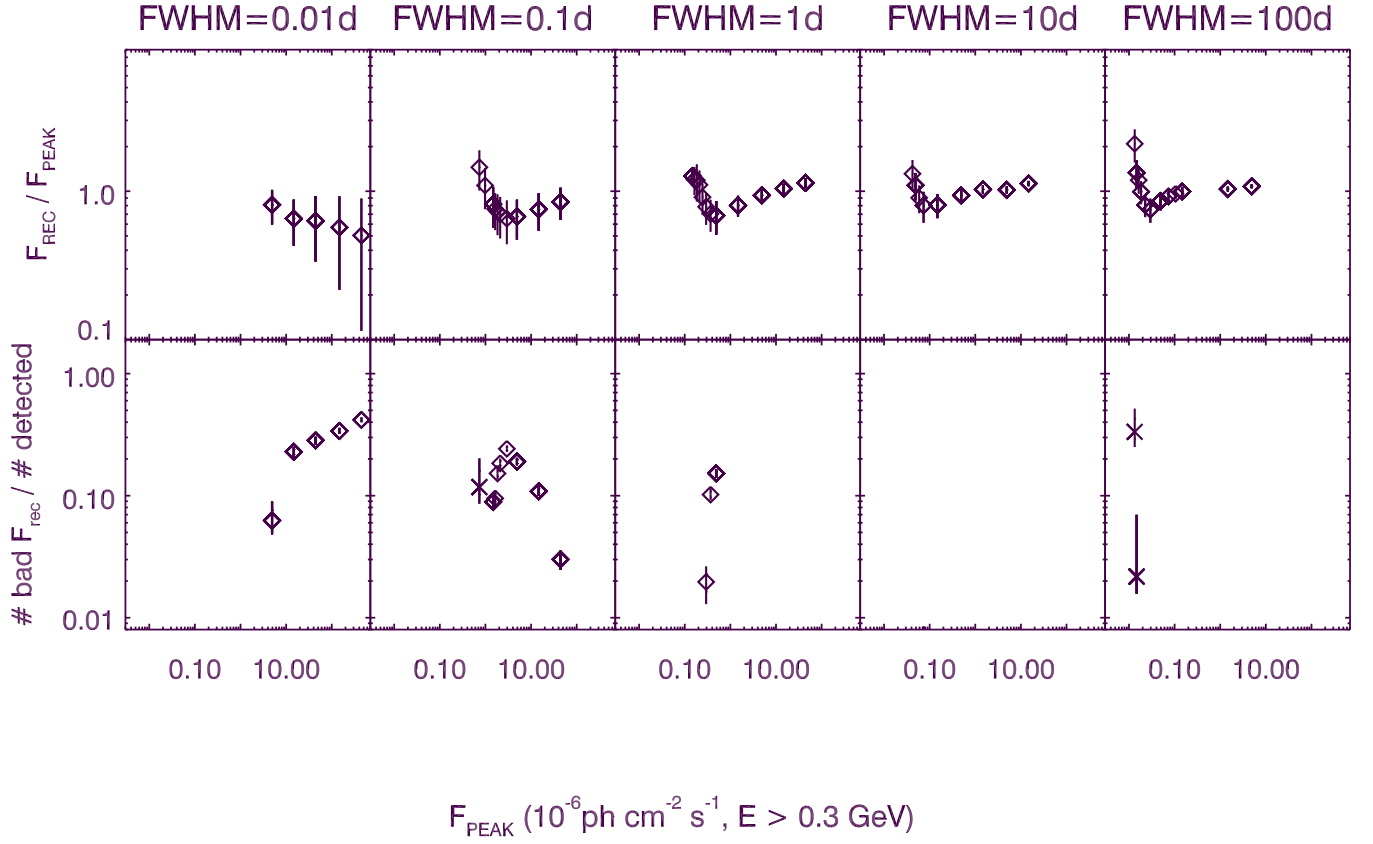


Fig. 5. Peak flux reconstruction capability. Top panels: Mean (open diamonds) and standard deviation (vertical lines) of the reconstructed flux (normalized to the simulated peak flux) is reported as a function of the peak flux for different values of the FWHM. Bottom panels: Number of flares (normalized to the number of detected flares) for which the reconstructed peak flux is below a factor $\frac{1}{2}$ of the simulated value (diamonds), or above a factor 2 of the simulated value (crosses). Where values are not reported in bottom panels, upper limits of 6.6% (with 99.87% c.l.) must be considered.

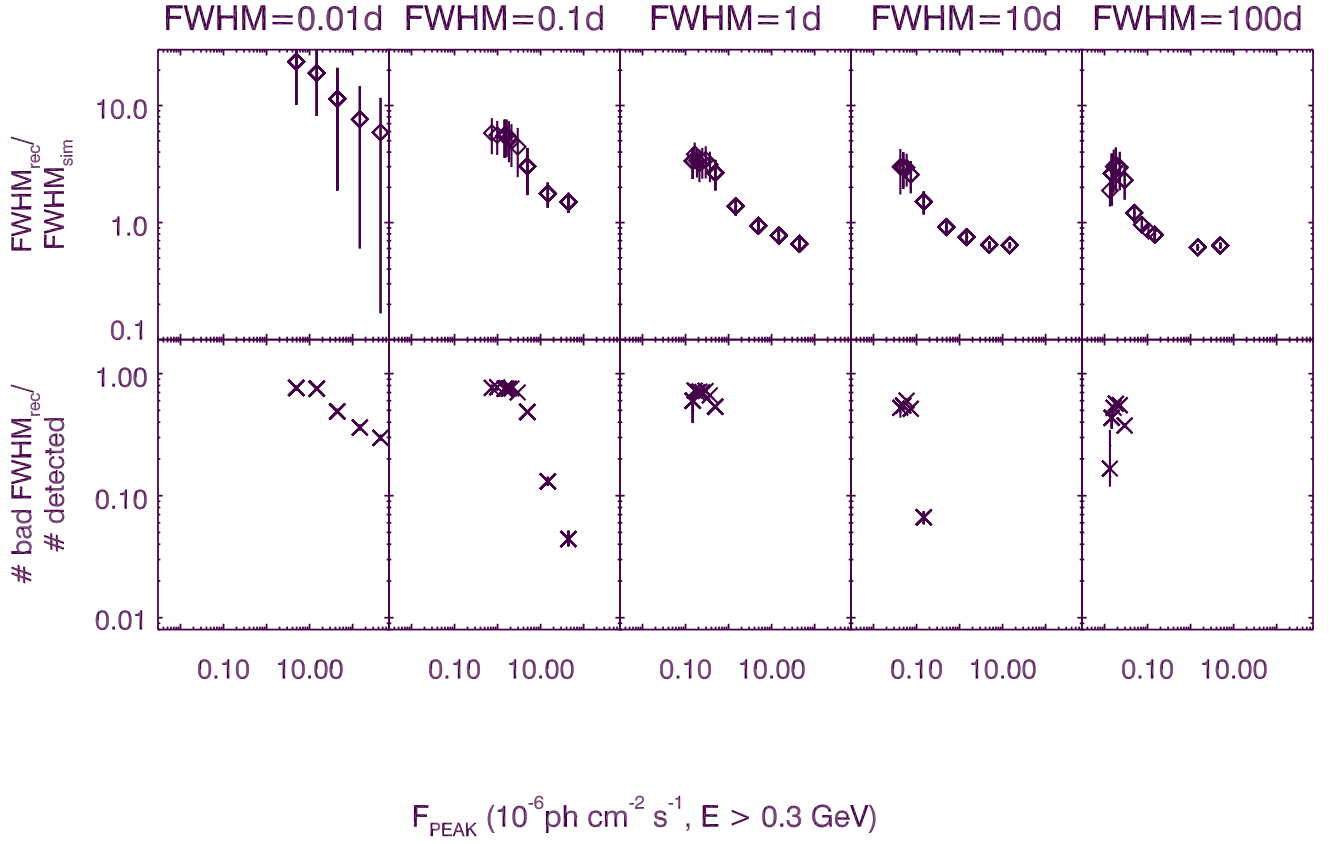


Fig. 6. Temporal FWHM reconstruction capability. Top panels: Mean (open diamonds) and standard deviation (vertical lines) of the reconstructed FWHM (normalized to the simulated FWHM) as a function of the peak flux for different values of the FWHM. Bottom panels: Number of flares (normalized to the number of detected flares) for which the reconstructed temporal FWHM is below a factor $\frac{1}{2}$ of the simulated value (diamonds), or above a factor 2 of the simulated value (crosses). Where values are not reported in bottom panels, upper limits of 6.6% (with 99.87% c.l.) must be considered.

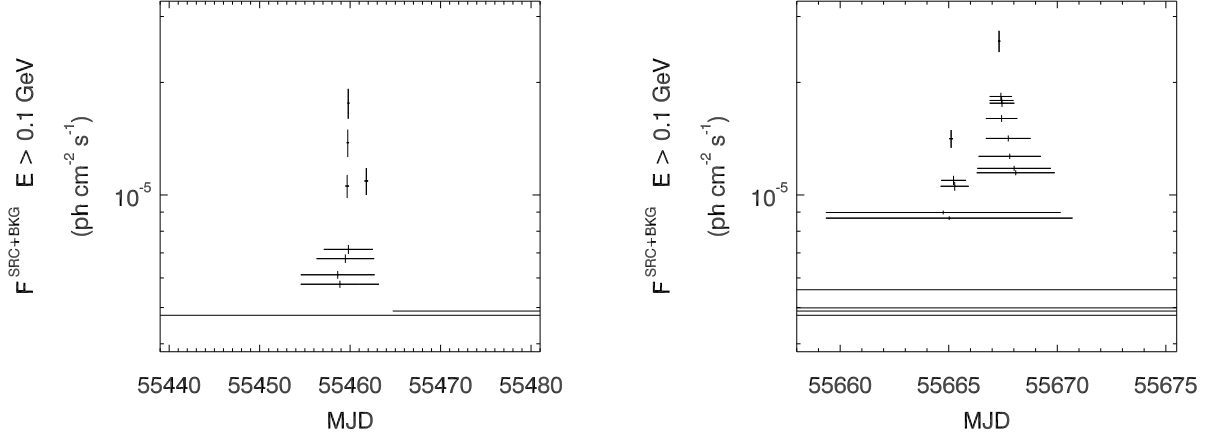


Fig. 7. Unbinned light curve for the Crab Nebula, obtained with $N_{tol} = 50$, $E > 0.1$ GeV, extraction radius corresponding to the containment of 68% of photons from the source. Confidence level is 99.87%. The unbinned light curve is produced for 7.25 y, but only two already studied periods are shown for a direct comparison of the results: Left panel reports the observing period investigated in Striani (2013) and in Abdo (2011a). Right panel reports the observing period investigated in Buehler (2012). Each horizontal segment represents a cluster: it subtends the temporal interval characterizing the cluster; its length is the length of the cluster in the temporal domain; its height is the mean photometric flux of the source within the subtended temporal interval. The unbinned light curve as a whole is a representation of a single-root tree like hierarchy. The bottom segment is the root cluster. Ascending the tree corresponds to go from the bottom up of the plotted diagram of clusters. For each cluster, a parent can be identified (the boundaries of a son cluster are within the boundaries of the parent). All the reported clusters which can be regarded as parents do not describe flat activity periods (the hypothesis that the events within a parent cluster are uniformly distributed is rejected with a confidence level of 99.87%). Clusters and chain of clusters are expected for flaring periods, when the hypothesis of uniformly distributed events is false. Leaves are the activity peaks. Every son cluster is statistically relevant with respect to its parent, according to the chosen confidence level. Therefore the unbinned light curve is a statistically filtered representation of the source activity.

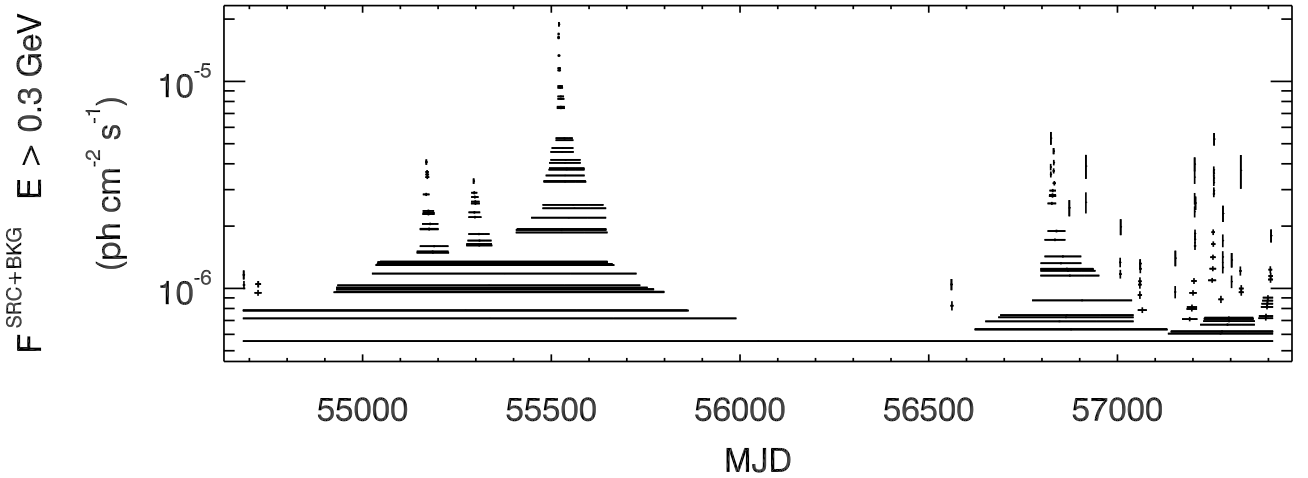


Fig. 8. Unbinned light curve for the Flat Spectrum Radio Quasar 3C 454.3, obtained with $N_{tol} = 50$, $E > 0.3$ GeV, extraction radius corresponding to the containment of 68% of photons from the source, 99.87% c.l.

Appendix A: Fragmentation artifact and the choice of N_{tol} parameter

In the proposed procedure, fragmentation is an artifact introduced with clustering: In the case of a period of flat source activity (with flux F_{flat}), the analyst expects to find a single cluster describing the flat period. The construction of clusters making use of eq. 1 lead to the subdivision of the flat period in several clusters. I call fragmentation this artifact. In fact, for $\Delta_{thr} \sim 1/F_{flat}$, we expect half of the exposure spacings among contiguous events to be larger than $1/F_{flat}$. The result is the constructions of several clusters during the flat period.

Fragmentation is not limited to periods of flat activity, but can occur also for flaring periods: If we have a flare, once we have chosen a value for Δ_{thr} , we expect to build a single cluster, but, due to the stochastic nature of the problem, several clusters can form.

The clustering scheme obeying eq. 2 reduces the occurrence of fragmentation provided that a suitable N_{tol} parameter is chosen. The evaluation of the occurrence of fragmentation is performed here with simulations, testing the proposed algorithm with three test-functions: trapezoidal, triangular, or the temporal shape described by equation 9. Background, and steady source activity is neglected. For the case of trapezoidal shape, the 80% of events are simulated within the flat period (the superior base of the trapezoid). I consider the cases that the instrument collects 400, 1600, 6400, $25 \cdot 10^3$, 10^5 photons during the activity period under examination. For each temporal shape, and each photon statistic, I run up to $3 \cdot 10^4$ simulations. Peaks are identified following the procedure proposed in this paper. The tolerance parameter is set to 1, 3, 5, 10, 25, 50, 100. Fragmentation appears if there is more than one detected peak for a simulated activity period (e.g., for a simulation). Results are shown in fig. A.1.

A tolerance parameter of 50 is suitable for flares with up to $25 \cdot 10^3$ events: with this choice fragmentation occurrence is at the level of 1% or less. Moreover this value is useful to describe large activity plateau with 10^5 events. For flaring periods of 10^3 events or less, a tolerance parameter of 1 could be chosen.

The following procedure is suggested to correctly choose the N_{tol} parameter: Obviously, fragmentation probability rises with the number of flare events, and it decreases while increasing N_{tol} . If we could know the number of events (N_f) of the activity periods, we could evaluate the fragmentation probability at a given N_{tol} and at the number of flare events corresponding to N_f for the worst case among the three test functions reported in fig. A.1. Then we could choose N_{tol} that keeps fragmentation probability at the desired level.

Before data analysis is performed, we do not know the number of events of each flare, but the total sample size is known. If the sample size is 10^3 events or less, the tolerance parameter can be set to $N_{tol} = 1$. This choice allows for the fragmentation artifact to be below 1% for each detected flare (from the worst case among the ones reported in fig A.1 for $N_{tol} = 1$).

For larger sample sizes, the suggested procedure is to prepare a preliminary unbinned light curve with the tolerance parameter set to a large value (e.g., $N_{tol} = 100$). From the set $\{C_i\}$ of clusters surviving the removal procedure, each son of the root contains all the events of one or more flares, and they are the clusters with the largest size. The analyst must choose the accepted cluster with the largest size (excluding the root). The number of events of this cluster (N^{max}) is equal or larger than the number of the events of the brightest flare. N^{max} can be used together with the fragmentation estimates reported in fig.

A.1 to choose the correct value for N_{tol} in order to maintain the fragmentation probability below a predefined level for each flaring period.

The obtained value of N_{tol} can be used to produce the final unbinned light curve.

As an example, if the analyst finds from the preliminary unbinned light curve that the cluster with the largest size (excluding the root) contains $25 \cdot 10^3$ events, from the three test functions reported in fig. A.1, he obtains that $N_{tol} = 50$ gives a fragmentation probability $\sim 0.7\%$ for the worst case (triangular shape flare). Thence, if a fragmentation probability $\sim 0.7\%$ is considered acceptable by the analyst, the final unbinned light curve can be prepared with $N_{tol} = 50$.

Appendix B: Multiple Flares resolving power

The proposed clustering scheme (eq. 2) avoids fragmentation artifact, provided that a suitable N_{tol} parameter is chosen.

If two contiguous flares are separated by more than $2N_{tol}$ events, the SRS clustering scheme do not merge them. If two contiguous flares are separated by no more than $2N_{tol}$ events, they could be glued together, a resolving power issue can arise: Flares are described by a chain of clusters. The two flares are roughly resolved if for each flare there exists at least a statistically relevant cluster (the cluster with the shortest Δ_{thr}) for which eq. 2 is not satisfied.

In figure B.1 I show the results of such an evaluation assuming 4700 background events uniformly distributed on an unitary segment. This background level corresponds to the background counts within a circular region of radius $R_{68}(type_i, E_i)$ around the FSRQ 3C 454.3 (see appendix D). Gluing effect is evaluated for two identical box shaped flares. The width of each box is denoted with L , the event density of the flare (the flare flux) is denoted with ρ_F , the background event density is denoted with ρ_0 . I assumed the case in which there are N_{tol} events in between the two box shaped flares (for a number of events larger than $2N_{tol}$ in between the two flares, there is no gluing). The glued cluster can have no more than $3N_{tol} + 2(\rho_F + \rho_0)L$ events, and have a size $\sim \frac{3N_{tol}}{\rho_0} + 2L$. I denote C_{glued} this cluster, and ρ_{glued} the mean event density of the glued cluster. I evaluated the minimum flare width (L_{min}) for which clusters of length L and $(\rho_F + \rho_0)L$ events are statistically relevant at 99.87% c.l. with respect to C_{glued} . The minimum L is reported in figure B.1 as a function of $\frac{\rho_F}{\rho_0}$. For comparison, I report in figure B.1 also the sensitivity limit for two identical box-shaped flares. For a single flare, sensitivity limit has an horizontal asymptote at $L = 1$. For two identical flares (such as in the present case), the horizontal asymptote is at $L = 1/2$ (top sensitivity limit curve).

For any given $\frac{\rho_F}{\rho_0}$, two identical flares are resolved until their width is larger than L_{min} . In the interval between L_{min} and the bottom sensitivity limit, the flares are detected as a single flare. There is a range of values of $\frac{\rho_F}{\rho_0}$ for which L_{min} is not defined. Within this range, the two identical flares are always resolved, if they are detectable above background.

The lower N_{tol} is set, the lower gluing is. The case $N_{tol} = 1$ corresponds to the simple clustering of eq. 1.

Appendix C: Fermi-LAT Data Preparation

I performed data preparation and likelihood analysis tasks using the standard Fermi Science Tools (v10r0p5), the PASS8

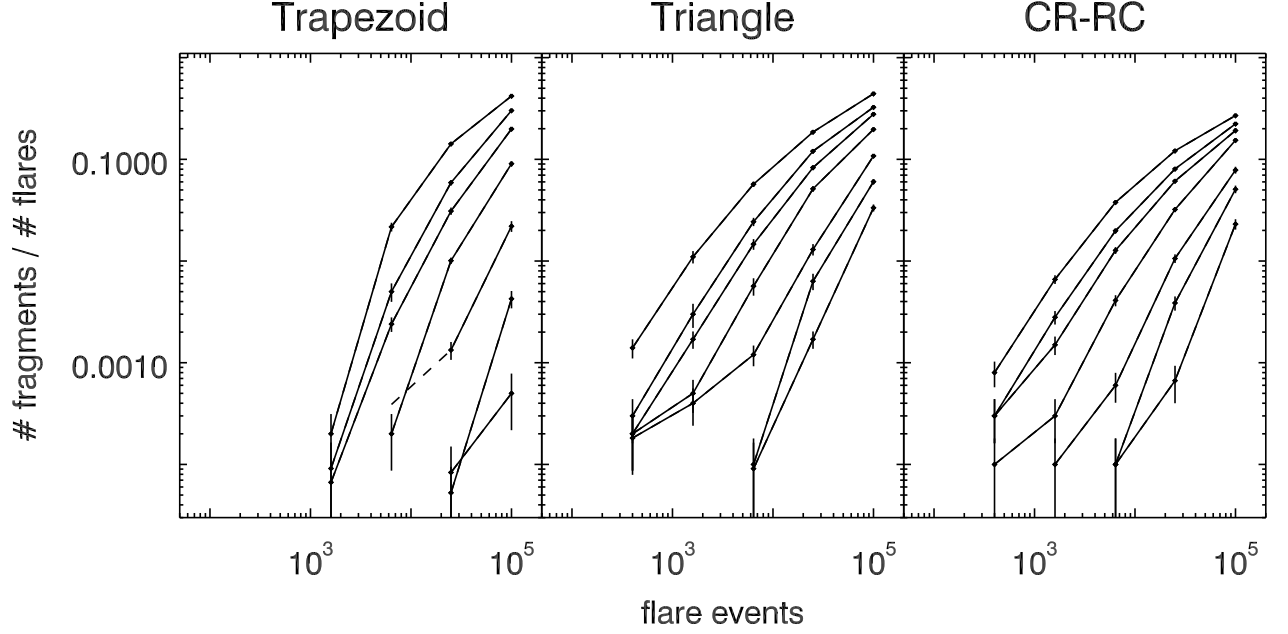


Fig. A.1. Frequency of Fragmentation artifact as a function of the events collected during the flaring period. The three panels are for the following temporal shapes: trapezoidal (left panel), triangular (central panel), temporal shape described in eq. 9 (right panel). The clustering scheme of eq. 2 is used. Continuous lines are used to connect the evaluated frequencies for the same tolerance parameter. Dashed lines are used to connect evaluated frequency to upper limits (99.87% c.l.). From top to bottom curves, tolerance parameters is set to 1, 3, 5, 10, 25, 50, 100.

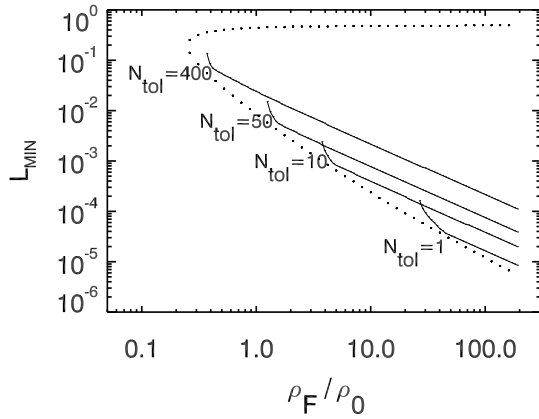


Fig. B.1. Resolving Power Capability for various N_{tol} parameters. Computation refers to two identical box shaped flares. L is the width of each flare; ρ_F if the event density of the flare. ρ_0 is the background event density. There are N_{tol} background events in between the two flares. The continuous curves represent the minimum flare width for which the two contiguous flares are resolved. Dotted curve is the sensitivity limit (99.87% c.l.) for two identical box shaped flares. For any given $\frac{\rho_F}{\rho_0}$ two identical flares of length lower than the computed values are not resolved.

Response Functions (P8R2_SOURCE_V6), and standard analysis cuts: The *gtselect* task was used to select SOURCE class events (evclass=128), collected within 20° from the investigated source. Earth's limb gamma-rays were rejected applying a zenith angle cut of 90° . To prepare input files to the likelihood procedure, only good-quality data, taken during standard data taking mode, were selected using the *gtmktime* task. Livetime cube was prepared taking into account the zenith angle cut. Exposure maps was prepared using standard recipes.

Unbinned likelihood analysis was performed including all the sources from the third Fermi-LAT catalog (Acero 2015) within the chosen region of interest (ROI).

For the investigated source and for sources within 10° from the ROI center, all the spectral parameters were allowed to vary. For all the other sources, only the normalization factor were allowed to vary.

To prepare input files to the *gtexposure* and to the SRS clustering procedure, GTIs were prepared with *gtmktime* task for good-quality data, taken during standard data taking mode, and for source events outside the Earth limb. The finely binned exposure with a binsize of 86.4 s was prepared with standard *gtexposure* tool, using the 3FGL catalog spectral template for the investigated source.

The filtered photon list is sorted with respect to time. The finely binned exposure, and the filtered photon-list are the inputs of the task of SRS clustering.

Appendix D: Background Level estimate

Between MJD 55800 and MJD 56100 the FSRQ 3C 454.3 underwent a period of extremely faint activity (see light curve in Pacciani 2014). The unbinned likelihood analysis performed above 0.3 GeV with a Region of Interest (ROI) of 20° for that period gives a source flux of $(0.75 \pm 0.13) 10^{-8} \text{ ph cm}^{-2} \text{ s}^{-1}$, 184 source events collected by the FERMI-LAT (Npred), and a source test statistics (ts) of 79.

The exposure to the source (evaluated using `gtexposure`) for that period is $2.5 \cdot 10^{10} \text{ cm}^2 \text{ s}$ ($E > 0.3 \text{ GeV}$).

There are 704 gamma-ray events collected above 0.3 GeV within $R_{68}(\text{type}_i, E_i)$ (defined in section 3) for the studied faint activity period. So I can assume 579 ± 45 background gamma-ray within $R_{68}(\text{type}_i, E_i)$. The FERMI-LAT exposure to the source for the 7.25 y period is $2.2 \cdot 10^{11} \text{ cm}^2 \text{ s}$ ($E > 0.3 \text{ GeV}$). The extrapolated background for the whole period is 5200 ± 400 counts.

Second method (multiple background regions method):

Background counts can be evaluated using a photometric method, using a suitable extraction region. But the background level varies with galactic coordinates, so I choose to extract background counts from 36 circular background regions. The centers of the circles are placed on a circumference of radius $R_c = 10^\circ$ centered on the position of the investigated source (3C 454.3). They are equally spaced on that circumference. the radius of circular background regions is dynamically chosen with the same criteria used for the definition of $R_{68}(\text{type}_i, E_i)$, but rescaled by a factor $f_{\text{rescale}} = 4$ with respect to $R_{68}(\text{type}_i, E_i)$. For each background circular region, we can identify an other background region which is located in the opposite direction in the reference frame centered on the investigated source. I refer these two as homologous regions.

The exposure of each circular background region differs to the other regions and to the exposure of the investigated source. The sky scanning strategy of the FERMI satellite mitigates differences. Moreover, the choice of multiple background regions further reduce differences in the effective area among the source region and the mean of the surrounding background regions. The usage of homologous regions brings to cancellation of differences.

The preparation of Fermi-LAT data for the SRS clustering handles Earth occultation, and discriminates Earth-albedo gamma-rays using zenith angle cuts in `gtselect` (see Cicerone web pages⁴).

The `gtmkttime` procedure is used to prepare GTIs to account for the occultation of the source region only. The satellite is in near equatorial orbit, therefore the Earth albedo and Earth occultation GTIs mainly depend on the celestial declination of each region. There are periods in which the background regions are not occulted by the Earth but are removed from the analysis with `gtmkttime` (this fact gives no systematic in the evaluation of background). Conversely, there are periods in which the background regions are occulted by the Earth (or collect Earth-albedo gamma-rays) and the Earth-albedo gamma-ray are filtered out with the `gtselect` procedure, but this filtering is not accounted for with `gtmkttime` (`gtmkttime` is used

to prepare the GTIs to filter-out periods for which the source is below the Earth limb). This fact is not taken into account in the background evaluation procedure. It gives a systematic in the evaluation of background. There are two extreme cases: The first is for background regions located at the same celestial declination of the source, and 10° apart in right ascension. for such background regions, the reduction of background counts is a factor $\frac{10^\circ}{360^\circ} \sim 2.8\%$. The detailed semi-analytical calculation, taking into account the satellite path along the Earth, shows that the average loss of background events (not accounted for in the built GTIs and in the exposure calculation) is $\sim 1.7\%$.

The second case is for regions at the same right ascension of the source, and the source at the edge of the Earth limb. In such a situation, there is a loss of background counts for the regions at the lower declination that is not accounted for by the exposure. The detailed calculation shows that the largest loss of events among regions is 22%, but the loss of counts involves less than half of the background regions. The average loss of background counts is 8.6%.

For the purpose of this paper, I disregard these systematics.

With this approximation and in the ideal case of no contaminating sources giving counts within the circular background regions, the background estimated performing the average of two homologous regions is a linear interpolation of the background level at the position of the investigated source.

In order to remove contaminating sources, the three regions with the largest counts, and their homologous are neglected. Moreover, the three regions with the shortest counts, and their homologous are neglected. The background level at the position of the investigated source is estimated as the average from the counts of the survived background circular regions (rescaled by a factor f_{rescale}^2).

Using this method, the background counts within a region of radius $R_{68}(\text{type}_i, E_i)$ centered at the position of 3C 454.3, during the extremely faint activity period, are: 540 ± 30 . This estimate is comparable with the first method. The extrapolated background for the 7.25 y period is 4880 ± 270 counts.

Using the multiple background regions method for the 7.25 y period, the background level within a region of radius $R_{68}(\text{type}_i, E_i)$ centered on the position of 3C 454.3, is 4680 ± 80 . The method of multiple background regions cannot be used for sources too close to the galactic plane, because in this case, the average of the counts within the background regions is not representative of the background at the position of the investigated source.

Acknowledgements. I am grateful to I. Donnarumma and A. Stamerra for discussions. L.P. acknowledges contribution from the grant INAF SKA-CTA.

References

- Abdo, A. A., et al. 2011 Sci, 331, 739
- Abdo, A. A., et al. 2011 ApJ, 733, L26
- Acero F., et al. 2015, ApJS, 218, 23
- Ackermann, M. et al. 2013, ApJ, 771, 57
- Atwood, W. B., et al. 2009, ApJ, 697, 1071
- Bateman, G., 1948, Biometrika, 35, 97
- Britto, R. J., Bottacini, E., Lott, B., Razzaque, S., Buson, S. 2016, ApJ, 830, 162
- Boutsikas, M. V., Koutras, M. V., Milienos, F. S. 2009, Scan Statistics - Methods and Applications, ed Glaz, J., Pozdnyakov, V. & Wallenstein, S Birkäuser (Boston), 55
- Buehler, J. D. et al, 2012, ApJ, 749, 26
- Bulgarelli, A., et al, 2012, AA, 538, 63
- Coogan, R. T., Brown, A. M., Chadwick, P. M. 2016 MNRAS, 458, 354
- Cucala, L 2008 Biometrical Journal, 50, 299

⁴ https://fermi.gsfc.nasa.gov/ssc/data/analysis/documentation/Cicerone/Cicerone_Likelihood/Exposure.html

(section: *Excluding Atmospheric Background Events*);

https://fermi.gsfc.nasa.gov/ssc/data/analysis/scitools/aperture_photometry.html;

https://fermi.gsfc.nasa.gov/ssc/data/analysis/scitools/data_preparation.html.

- Glaz, J., Naus, J., Roos, M., Wallenstein, S. 1994, *Journal of Applied Probability*, 31, 271
- Glaz, J. & Zhang, Z., 2006, *Statistics & Probability Letters*, 76, 1316
- Haiman, G. & Preda, C. 2009, *Scan Statistics - Methods and Applications*, ed Glaz, J., Pozdnyakov, V. & Wallenstein, S Birkäuser (Boston), 179
- Huffer, F., 1997, *Journal of the American Statistical Association (JASA)*, 92, 1466
- Huffer, F., & Lin, C. T. 1997, *Journal of the American Statistical Association (JASA)*, 92, 1466
- Huntington R. J. & Naus, J. 1975, *The Annals of Probability*, 3, 894
- James, F. 1990, *Comput. Phys. Commun.*, 60, 329
- Lott, B., Escande, L., Larsson, S., & Ballet, J. 2012, *A&A*, 544, 6
- Marsaglia, G., Zaman, A., Tsang W. W., 1990, *Stat. Prob. Lett.* 9, 35
- Mattox, J. R. et al. 1996, *ApJ*, 461, 396
- McConville, W. F. et al. 2011 *ApJ*, 738, 148
- Nagarwalla, N., 1996, *Statistics in Medicine*, 15, 845
- Nauss J. I., 1965, *J. Amer. Statist. Assoc.*, 60, 532
- Nauss J. I., 1966, *Technometrics*, 8, 493
- Pacciani, L. et al. 2014, *ApJ*, 790, 45
- Pittori, C. et al. 2009, *AA*, 506, 1563
- Prahl, J. , arxiv: 9909389
- Reyes, L. C. and Cheung C. C., 2009, *ATel* #2226
- Scargle, J. D., 1998, *ApJ*, 504, 405
- Scargle, J. D., Norris, J. P., Jackson B., Chiang J., 1998, *ApJ*, 504, 405
- Striani, E. et al., 2013, *ApJ*, 765, 52
- Tavani, M., et al. 2009, *A&A*, 502, 995
- Tavani, M., et al. 2011 *Sci*, 331, 736
- Wallenstein, S 2009, *Scan Statistics - Methods and Applications*, ed Glaz, J., Pozdnyakov, V. & Wallenstein, S Birkäuser (Boston), 2